diabetes®
American Diabetes Association®

Protease-Activated Receptor 1–Mediated Damage of Podocytes in Diabetic Nephropathy

Ruslan Bohovyk, Sherif Khedr, Vladislav Levchenko, Mariia Stefanenko, Marharyta Semenikhina, Olha Kravtsova, Elena Isaeva, Aron M. Geurts, Christine A. Klemens, Oleg Palygin, and Alexander Staruschenko

Diabetes 2023;72(12):1795–1808 | https://doi.org/10.2337/db23-0032

Protease-Activated Receptor 1 Mediated Damage of Podocytes in Diabetic Nephropathy

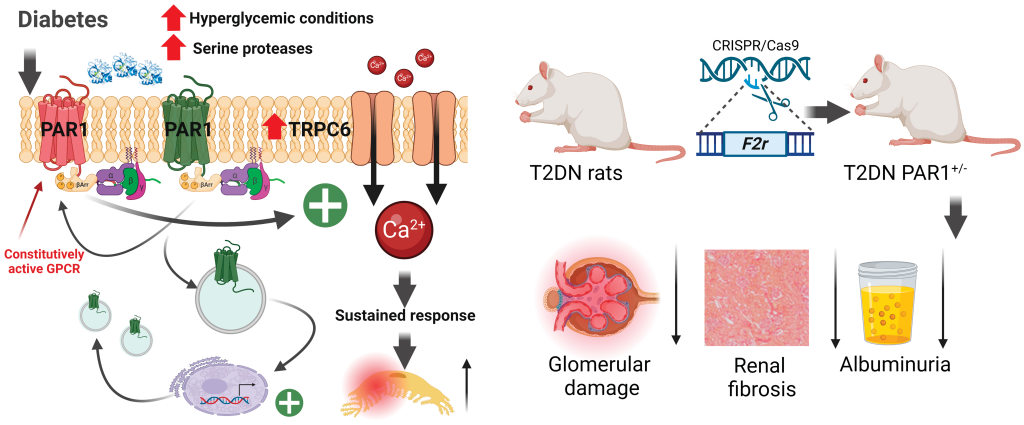

Conclusion:

During the development of diabetic neuropathy, elevated levels of serine proteases promote an excessive $[Ca^{2+}]_i$ influx in podocytes through the PAR1 G protein–coupled receptor (GPCR) mechanisms, ultimately leading to podocyte apoptosis, the development of albuminuria, and glomeruli damage.

Protease-Activated Receptor 1–Mediated Damage of Podocytes in Diabetic Nephropathy

Ruslan Bohovyk,[1] Sherif Khedr,[2] Vladislav Levchenko,[1] Mariia Stefanenko,[3] Marharyta Semenikhina,[3] Olha Kravtsova,[1] Elena Isaeva,[4] Aron M. Geurts,[4] Christine A. Klemens,[1,5] Oleg Palygin,[3,6] and Alexander Staruschenko[1,5,7]

Diabetes 2023;72:1795–1808 | https://doi.org/10.2337/db23-0032

There is clinical evidence that increased urinary serine proteases are associated with the disease severity in the setting of diabetic nephropathy (DN). Elevation of serine proteases may mediate $[Ca^{2+}]_i$ dynamics in podocytes through the protease-activated receptors (PARs) pathway, including associated activation of nonspecific cation channels. Cultured human podocytes and freshly isolated glomeruli were used for fluorescence and immunohistochemistry stainings, calcium imaging, Western blot analysis, scanning ion conductance microscopy, and patch clamp analysis. Goto-Kakizaki, Wistar, type 2 DN (T2DN), and a novel PAR1 knockout on T2DN rat background rats were used to test the importance of PAR1-mediated signaling in DN settings. We found that PAR1 activation increases $[Ca^{2+}]_i$ via TRPC6 channels. Both human cultured podocytes exposed to high glucose and podocytes from freshly isolated glomeruli of T2DN rats had increased PAR1-mediated $[Ca^{2+}]_i$ compared with controls. Imaging experiments revealed that PAR1 activation plays a role in podocyte morphological changes. T2DN rats exhibited a significantly higher response to thrombin and urokinase. Moreover, the plasma concentration of thrombin in T2DN rats was significantly elevated compared with Wistar rats. $T2DN^{Par1-/-}$ rats were embryonically lethal. $T2DN^{Par1+/-}$ rats had a significant decrease in glomerular damage associated with DN lesions. Overall, these data provide evidence that, during the development of DN, elevated levels of serine proteases promote an excessive $[Ca^{2+}]_i$ influx in podocytes through PAR1-TRPC6 signaling, ultimately leading to podocyte apoptosis, the development of albuminuria, and glomeruli damage.

ARTICLE HIGHLIGHTS

- Increased urinary serine proteases are associated with diabetic nephropathy.
- During the development of diabetic nephropathy in type 2 diabetes, the elevation of serine proteases could overstimulate protease-activated receptor 1 (PAR1).
- PAR1 signaling is involved in the development of DN via TRPC6-mediated intracellular calcium signaling.
- This study provides fundamental knowledge that can be used to develop efficient therapeutic approaches targeting serine proteases or corresponding PAR pathways to prevent or slow the progression of diabetes-associated kidney diseases.

The National Diabetes Statistics Report in 2022 found that nearly 37.3 million Americans (just over 1 in 10) have diabetes and 96 million American adult (approximately 1 in 3) have prediabetes. Diabetes-associated kidney diseases (DKDs), such as diabetic nephropathy (DN), are potential complications characterized by a gradual decrease in renal function (1,2). DN is the leading cause of end-stage renal failure, increasing as a national and global care problem. The characteristic pathological

[1]Department of Molecular Pharmacology and Physiology, University of South Florida, Tampa, FL
[2]Department of Physiology, Faculty of Medicine, Ain-Shams University, Cairo, Egypt
[3]Department of Medicine, Division of Nephrology, Medical University of South Carolina, Charleston, SC
[4]Department of Physiology, Medical College of Wisconsin, Milwaukee, WI
[5]Hypertension and Kidney Research Center, University of South Florida, Tampa, FL
[6]Department of Regenerative Medicine and Cell Biology, Medical University of South Carolina, Charleston, SC
[7]James A. Haley Veterans' Hospital, Tampa, FL
Corresponding author: Alexander Staruschenko, staruschenko@usf.edu

Received 10 January 2023 and accepted 4 September 2023
This article contains supplementary material online at https://doi.org/10.2337/figshare.24143136.

changes of DN include severe albuminuria, renal hyperfiltration, glomerular basement membrane (GBM) thickening, and glomerulosclerosis (3). Albuminuria is associated with pathological damage to the glomerular filtration barrier, which comprises three layers: glomerular endothelial cells, GBM, and glomerular visceral epithelial cells (podocytes) (4,5). Podocytes are terminally differentiated glomerular epithelial cells whose interdigitating foot processes form a significant component of the GBM. Therapeutic interventions targeting podocytes have become a major focus for diseases like DN because of their crucial role in regulating glomerular permeability and maintaining glomerular structures through interactions with other glomerular parenchymal cells, including endothelial cells (6).

Intracellular calcium ($[Ca^{2+}]_i$) signaling is involved in multiple mechanisms, including podocyte foot process formation and retraction, cell motility, and cells' ability to regulate the glomerular filtration barrier. The ability of $[Ca^{2+}]_i$ signaling in podocytes to regulate glomerular tuft contraction and capillary albumin permeability was previously reported (4,7). Changes in podocytes $[Ca^{2+}]_i$ can be initiated by G protein–associated signaling cascades such as activation of protease-activated receptors (PARs).

The four known members of the PAR family are the G protein–coupled receptors (GPCRs) that are activated by N-terminal proteolytic cleavage. This cleavage can be catalyzed by traditional serine proteases such as thrombin (for PAR1, PAR3, and PAR4) and trypsin (PAR2), as well as kallikrein or urokinase (8–10). Coagulation protease and PARs are widely expressed in renal cell types, such as tubular epithelial cells or podocytes (11,12). PARs are attractive, new therapeutic targets with pharmacological inhibitors currently available, such as vorapaxar, which the Food and Drug Administration approved in 2014 to reduce the risk of myocardial inflation, stroke, and cardiovascular death (13). Recent studies demonstrated that PARs could play a role in the glomerular, microvascular, and inflammatory regulation of renal function in normal and pathological conditions (11,14). Additional studies have also shown that PAR1 deficiency protects against streptozotocin (STZ)-induced DN and plays an essential role in developing DKD (15). Aberrant PAR signaling could potentially result in pathological $[Ca^{2+}]_i$ levels, leading to podocyte damage and death. Furthermore, there is clinical evidence that urinary serine protease levels are increased during diabetes, which likely activates PAR signaling; however, the downstream effect of signaling through PARs is not well established.

It was proposed that the downstream PAR signaling cascade, as well as other GPCRs, could involve transient receptor potential canonical (TRPC) channel activation, β-arrestin recruitment, Rho-dependent cytoskeleton rearrangement, activation of protein kinase C, and more (16,17). Furthermore, it was reported that inhibition of PAR1 ameliorated podocyte injury in a mouse model of nephropathy via reduced TRPC-mediated calcium entry, suggesting TRP channel opening may be triggered by PAR activation (18). Recent studies further revealed that podocyte PAR1 activation is a key initiator of human nephrotic syndrome circulating factor and that the PAR1 signaling effects were partly modulated through TRPC6 (19). The contribution of podocyte integrin-β3 and activated protein C in PAR1-dependent RhoA activation in podocytes was also recently demonstrated (20). However, further investigation into the molecular pathogenesis of PAR activation in podocytes and its role in DN is needed to determine whether PARs antagonism may be a treatment option for DKD.

Here we used several unique rat models, including a type 2 DN (T2DN) rat and a novel PAR1 knockout in T2DN background and podocyte culture, to explore the functional role of PAR1 in podocytes under DN settings. We found that PAR1 is highly expressed in podocytes, and its activation results in GPCR-induced extensive calcium influx in podocytes via TRPC6 channels. In conclusion, our results suggest that increased PAR1 activity via TRPC6-mediated $[Ca^{2+}]_i$ overload contributes to pathological remodeling in DN, and inhibition of this pathway may be a valuable clinical strategy to improve patient outcomes.

RESEARCH DESIGN AND METHODS

Animals

The animal use and welfare procedures adhered to the National Institutes of Health Guide for the Care and Use of Laboratory Animals, following protocols reviewed and approved by the Medical College of Wisconsin (MCW) Institutional Animal Care and Use Committee, Milwaukee, WI. Goto-Kakizaki (GK) (type 2 diabetic), Wistar (nondiabetic), and T2DN rats were used for experiments. The T2DN PAR1$^{+/-}$ rat (T2DN-F2r^{em1Mcwi}; Rat Genome Database ID: 5887111) was created at the MCW Gene Editing Rat Resource Center using CRISPR/Cas9 gene editing on the T2DN rat strain background. The gene editing resulted in a 2–base-pair frame shift deletion in exon 7 (Supplementary Fig. 1). Rats were maintained on an in-house standard diet (no. 50001, LabDiet; Purina), and water and food were provided ad libitum. At the age of 12 and >48 weeks, rats were anesthetized, and kidneys were flushed with phosphate-buffered saline via aortic catheterization as previously described. Terminal experiments were performed at the same time of day, between 12:00 P.M. and 3:00 P.M. For each rat, the left kidney was either snap-frozen or used for glomeruli isolation and Western blot analysis. The right kidney was placed in 10% formalin for histological studies. Urine samples were used to determine albumin levels by a fluorescent assay (Albumin Blue 580 dye; Molecular Probes, Eugene, OR) or urokinase (ELISA Kit #LS-F40596; LSBio, Seattle, WA). All rats used in the experiments were male, with the exception of a few instances where female groups were used and noted in the results.

Histological Staining and Analysis of Kidney Injury

Rat kidneys were formalin fixed, paraffin embedded, sectioned, and mounted on slides as previously described (21).

Slides were stained with Masson trichrome stain and used to detect fibrosis and glomerular damage. Fibrosis was assessed using color deconvolution and thresholding in Fiji image processing package (ImageJ 1.51u; National Institutes of Health). A glomerular damage score was performed using morphometric analysis based on a scale of 0–4, and an average score was calculated for each as described previously (22). For experiments with human tissue, human kidneys were obtained from an organ procurement company, where they were harvested with the intent to be used for transplantation, but were not used and were destined to be discarded. The kidneys were stored in a transplant preservation University of Wisconsin Solution (UW) solution (ViaSpan) on ice before the glomeruli isolation as described (23).

For immunofluorescence labeling, freshly isolated human or rat glomeruli was collected using a vibrodissociation approach (23) or sieving methods (24). These glomeruli were then fixed with chilled 4% paraformaldehyde in PBS with 1 mmol/L $CaCl_2$ and 2 mmol/L $MgCl_2$ for 20 min and then gently washed three times with ice-cold PBS. Next, the glomeruli were probed with PAR1 (1:100, #251324; Abbiotec, Escondido, CA) and nephrin (1:100; #sc-377246; Santa Cruz Biotechnology, Dallas, TX) antibodies. The following day, the glomeruli were washed three times with cold PBS and incubated with Alexa fluorophore–labeled secondary antibody (1:500; ThermoFisher, Pittsburgh, PA) in 2% BSA-PBS at room temperature in the dark. After three PBS washes, the glomeruli were incubated with 0.5 μg/mL Hoescht nuclear stain in PBS for 10 min at room temperature in the dark. After five final washes with PBS, the tissue was preserved, and the coverslip was mounted with Fluoromount-G (SouthernBiotech, Birmingham, AL). Z-stack images with 2-μm z-steps were captured on a confocal Nikon A1R inverted microscope using a Plan Apo 40×/NA 0.95 DIC M N2 objective by Nikon Elements AR software (Nikon, Tokyo, Japan). Postimage processing was performed with the Fiji image processing package.

Western Blotting

Isolated glomeruli or cultured human podocyte lysates were prepared as previously described. The glomeruli or cells were pulse sonicated in Laemmli buffer in the presence of a protease and phosphatase inhibitor cocktail (Roche, Mannheim, Germany) to achieve a final protein concentration of 20 mg/mL, and spin cleared at 10,000*g* for 10 min. The supernatant was subjected to SDS-PAGE, and transferred onto nitrocellulose membrane (Millipore, Bedford, MA) for antibody hybridization. Changes in protein expression were assessed using primary antibodies against PAR1 (1:100, #251324; ABBIOTEC, Escondido, CA); TRPC6 (1:1,000, #sc-515837; Santa Cruz Biotechnology), p-ERK1/2 (1:1,000, #36-8800; Thermo Fisher Scientific, Waltham, MA), and PLC-γ1 (1:1,000, #sc-7290; Santa Cruz Biotechnology). The secondary antibody was Goat Anti-Mouse (#1706516) or Goat Anti-Rabbit (#1706515) IgG (H + L)-HRP conjugate antibodies (1:1,000; Bio-Rad, Hercules, CA). Immunoreactive proteins were detected by the ChemiDoc imaging system (Bio-Rad). Quantification of Western blot bands was performed by densitometry using Image Lab 6.1 Software (Bio-Rad) and normalized to loading controls actin (I-19) (1:1,000, sc-1616, 1:10,000, #G1316; Santa Cruz Biotechnology, Dallas, TX) and β-tubulin (1:10,000, No. AC030; ABclonal, Woburn, MA).

Intracellular $[Ca^{2+}]_i$ Measurements in Cultured Human Podocytes and in Podocytes of Freshly Isolated Glomeruli

For confocal microscopy, we used conditionally immortalized human podocyte cell line AB 8/13 provided by M. Saleem (University of Bristol, Bristol, U.K.) that has been described previously (25). Cells were cultured on glass-bottomed dishes (no. 0 coverslip; Mattek) in an RPMI-1640 (Gibco) medium supplemented with 10% heat-inactivated FBS (Corning) and insulin-transferrin-selenium supplement (Gibco), with penicillin-streptomycin (Cytiva). Cells were taken 12–14 days after thermoswitching. For high-glucose treatment, 20 mmol/L glucose was added to cell media for 12 h to get the final glucose concentration in media of 30 mmol/L (26). Then cells were loaded with Fluo-8 (#21090; AAT Bioquest) fluorescent dye and incubated at 37°C for 1 h. Cells were rinsed, and media was replaced with bath solution (145 mmol/L NaCl, 4.5 mmol/L KCl, 2 mmol/L $CaCl_2$, 2 mmol/L $MgCl_2$, 10 mmol/L HEPES, pH 7.35). Records were obtained using the laser scanning confocal microscope system (Leica HCX PL APO CS 40×/NA 1.25 Oil) and analyzed using the Fiji image processing package.

Calcium levels in glomeruli podocytes were determined by using a laser scanning confocal microscope (Nikon A1-R, Plan Apo 20×/NA 0.75 and 60×/NA 1.4 Oil) as described previously (27). Freshly isolated, decapsulated glomeruli of perfused kidneys were incubated with Fluo-4 (5 μmol/L; excitation 488, emission 520/20 nm; #20190588; Invitrogen, Waltham, MA) and Fura 2-TH (5 μmol/L; excitation 488, emission >600 nm; #7196; Setareh Biotech, Eugene, OR) fluorescent dyes for 40 min at room temperature on a rotating shaker. Fluorescence intensity ratios (Fluo-4/Fura 2-TH) recordings and changes in intracellular $[Ca^{2+}]_i$ influx in podocytes were calculated. PAR1-activating peptides TFLLR-NH_2 or TRAP-6 (#1464 and #3497; Tocris Bioscience), PAR1 selective inhibitor RWJ 56100 (#2614; Tocris Bioscience), thrombin (#T6884; Sigma-Aldrich), urokinase (#ab92604; Abcam), and TRPC6 blocker SAR7334 (#5831; Tocris Bioscience) were applied to the podocytes of freshly isolated glomeruli in diabetic T2DN, GK, and control Wistar rats or cultured human podocytes to test changes in $[Ca^{2+}]_i$ influx.

Patch Clamp Recordings

Patch clamp electrophysiology was used to assess channel activity in freshly isolated glomeruli. Single-channel current data were acquired as described previously (28). All electrophysiological recordings were performed using a physiological saline solution as the extracellular bath. Solution composition was (in mmol/L) 126 NaCl, 1 $CaCl_2$, 2 $MgCl_2$, 10 glucose, and 10 HEPES (pH 7.4). TRPC activity was recorded on the glomeruli using patch pipettes filled with a solution of the

following composition (in mmol/L): 126 NaCl, 1.5 $CaCl_2$, 10 glucose, and 10 HEPES (pH 7.4); 100 μmol/L niflumic acid or DIDS (4,4′-diisothiocyanato-2,2′-stilbenedisulfonic acid disodium salt), 10 mmol/L TEA (tetraethylammonium chloride), 10 nmol/L iberiotoxin, and 10 μmol/L nicardipine were added directly before the patch clamp experiment to block the activity of endogenous channels, which are not relevant for the studies. Resistance of patch pipettes ranged from 8 to 10 mol/LΩ. Gap-free single-channel current data from giga-ohm seals in principal cells were acquired and subsequently analyzed with Clampfit 10.7 software (Molecular Devices).

Scanning Ion Conductance Microscopy

The effect of PAR1 receptor agonists on podocyte structure was visualized by scanning ion conductance microscopy (SICM). For this purpose, the custom-modified scanner ICNano (ICAPPIC Ltd., London, U.K.) was used, and scanning was performed as described (29). Briefly, fine-tipped scanning nanopipettes were pulled from borosilicate glass (outer diameter/internal diameter: 1/0.5 mm) with the horizontal laser puller P-97 (Sutter Instruments). The pipette resistance was 80–100 mol/LΩ, corresponding to an estimated 90- to 120-nm tip diameter. Nanopipettes were held in voltage clamp mode with an Axopatch 700B patch clamp amplifier (Axon Instruments). The scan system was mounted on a Nikon TE2000-U inverted microscope (Nikon Instruments). Raw data were processed using SICM ImageViewer microscopy analysis software (ICAPPIC).

Statistics

Data are presented as mean ± SEM. In the box plot graphs, the box represents the mean ± SEM. Data were tested for normality (Shapiro-Wilk) and equal variance (Levene homogeneity test). Statistical analysis consisted of one- or two-way ANOVA or Student *t* test (OriginPro 9.0 or GraphPad Prism 9.0), with a *P* value of <0.05 considered significant. In addition, when an ANOVA test was significant, post hoc Holm-Sidak multiple comparison was performed.

Data and Resource Availability

All data used in the study are available in this article. Raw data may be provided by the corresponding author upon request.

RESULTS

PAR1 Is Expressed in Human Podocytes

Here, we first tested the expression of PAR1 in freshly isolated human glomeruli. Figure 1*A* shows a representative microphotograph of a human glomerulus with immunofluorescent labeling of the podocyte marker nephrin colocalizing with PAR1. To further explore the possible involvement of PAR1 signaling in diabetes, we used immunostaining of the kidney samples from patients without diabetes and with type 2 diabetes. Figure 1*B* shows that PAR1 expression was increased in the diabetic kidney and, overall, reveals higher expression in podocyte and distal tubules. We have performed a semiquantitative analysis of PAR1 staining by estimating changes in expression using samples from three subjects in each group. Our analysis revealed increased protein expression levels in the group with diabetes compared with the group without diabetes (11.2 ± 3.7 vs. 21.7 ± 6%, $n \geq 29$ regions of interest, $N = 3$ samples, $P < 0.001$).

Hyperglycemia-Induced Increase in PAR1 Response in Cultured Human Podocytes

We use human podocyte cells exposed to high glucose to estimate the changes in PAR1-mediated signaling in hyperglycemic conditions. After 12-h incubation in control or high-glucose solutions, cells were loaded with the fluorescent dye, and live-cell calcium imaging was performed. High-glucose–treated cells demonstrated a significant increase of $[Ca^{2+}]_i$ in response to a PAR1-specific agonist (TFLLR-NH_2) (Fig. 2*A* and *B*). The increase in amplitude and total $[Ca^{2+}]_i$ response (determined by the area under the curve) suggests a substantial calcium overload, which is a key determinant of podocyte apoptotic response (Fig. 2*C*). Experiments with iso-osmolar control for the high-glucose condition (mannitol) confirmed that the increase in osmolarity, specifically the 20-mOsm/kg difference, does not affect the calcium response in podocytes. Additionally, we found that calcium response was significantly lower in both the control group and the high-glucose group in the calcium-free solution. These findings suggest that PAR-mediated calcium responses are predominately mediated via activation of the plasma membrane calcium channels (Supplementary Fig. 2*A* and *B*). Furthermore, we observed no significant alterations in PAR1 expression in podocytes following a 12-h incubation under high-glucose conditions (Supplementary Fig. 2*C*). The specificity of the PAR1 signaling activation in podocytes was confirmed by the addition of PAR1 receptor blocker RWJ 56100 (Fig. 2*D*). As shown in Fig. 2*D*, PAR1 antagonist blocked the PAR-mediated calcium response (1,650 ± 129 vs. 368 ± 67 arbitrary units [a.u.], for TFLLR vs. TFLLR+RWJ, $n \geq 25$ cells, $^{***}P < 0.001$), confirming direct PAR1 involvement in Ca^{2+} flux in podocytes.

PAR1-Mediated Remodeling of Podocyte Structures

The following experiments revealed significant changes in cell structure in response to PAR1-mediated intracellular Ca^{2+} influx. The transmitted light images from experiments show rapid podocyte cell junction retraction in response to PAR1 agonist application (Fig. 3*A*). To quantify structural changes in cultured human podocyte lamellipodium growth and retraction, we used SICM. SICM allowed us to record nanometer-resolution 3D topographical images of lamellipodium at different time points before and after activation of PAR1 signaling (Fig. 3*B* and Supplementary Video 1). The normal growth of the lamellipodia is altered by the PAR1 activation; moreover, it led to significant retraction of the lamellipodium and a decrease in cell surface area (+51 ± 46 vs. −15 ± 8 μm^2, 30 min after application of vehicle or TFLLR-NH_2, respectively; $n = 5$, $P < 0.05$) (Fig. 3*C*). These

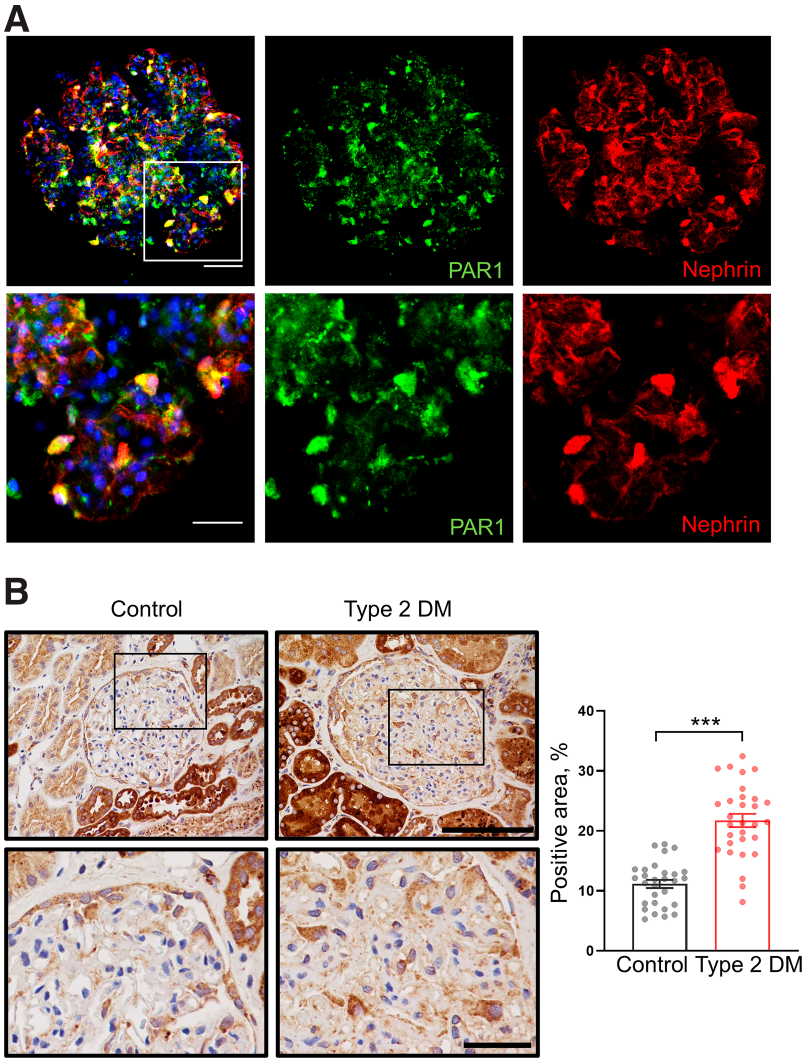

Figure 1—PAR1 expression in human glomeruli. *A*: Expression of PAR1 in human podocytes. Representative microphotograph of decapsulated human glomerulus freshly isolated from kidney cortex. Immunolabeling demonstrates colocalization of PAR1 (green) and nephrin (red; podocyte-specific marker) proteins. Cell nuclei are blue. Merged and separate confocal images for PAR1 and nephrin are shown (top: scale bar is 50 μm; bottom, scale bar is 25 μm). *B*: Immunostaining for PAR1 expression of control and diabetic samples (top, scale bar is 100 μm; bottom, scale bar is 25 μm). Black rectangles in the top images highlight the specified areas, which are zoomed-in in the bottom images, demonstrating the PAR1 expression in glomeruli. Summary of protein expression levels in the group without diabetes compared with the group with diabetes (11.2 ± 3.7 vs. 21.7 ± 6%, $n \geq 29$ regions of interest, $N = 3$ samples, $^{***}P < 0.001$).

data provide evidence that PAR1 activation plays a role in podocyte morphological changes.

Downstream Signaling Changes in Cultured Human Podocytes After PAR1 Activation

Activation of PARs and transient receptor potential canonical type 6 (TRPC6) channels can trigger different downstream signaling involved in cytoskeletal reorganization (29,30). Moreover, it was reported that different mitogen-activated protein kinases (MAPK) could be involved in the progression of various glomerulopathies and podocyte injury. Specifically, activation of p38 MAPK is a critical upstream mechanism for podocyte injury (31). Thus, in order to determine specific signaling pathways involved in PAR1 activation, we measured the expression of key proteins and their phosphorylation over time in cultured human podocytes following PAR1 activation. These experiments were conducted on cells not pretreated with high glucose. Figure 4 depicts the Western blots and summarized changes in the expression of PAR1, TRPC6, phosphorylated extracellular signal-regulated kinase 1/2 (p-ERK1/2), and phospholipase C γ (PLC-γ1). Stimulation of the PAR1 receptor intracellular cascade via the specific peptide TFLLR-NH_2 promoted a remodeling in the activation and/or expression of proteins proposed to be downstream of PAR1 signaling (Fig. 4). Treatment with a PAR1 agonist resulted in an initial elevation of PAR1 expression within the first 30 min, followed by internalization and lysosomal degradation in 2–4 h (typical for PARs). This decrease in PAR1 was accompanied by an increase in

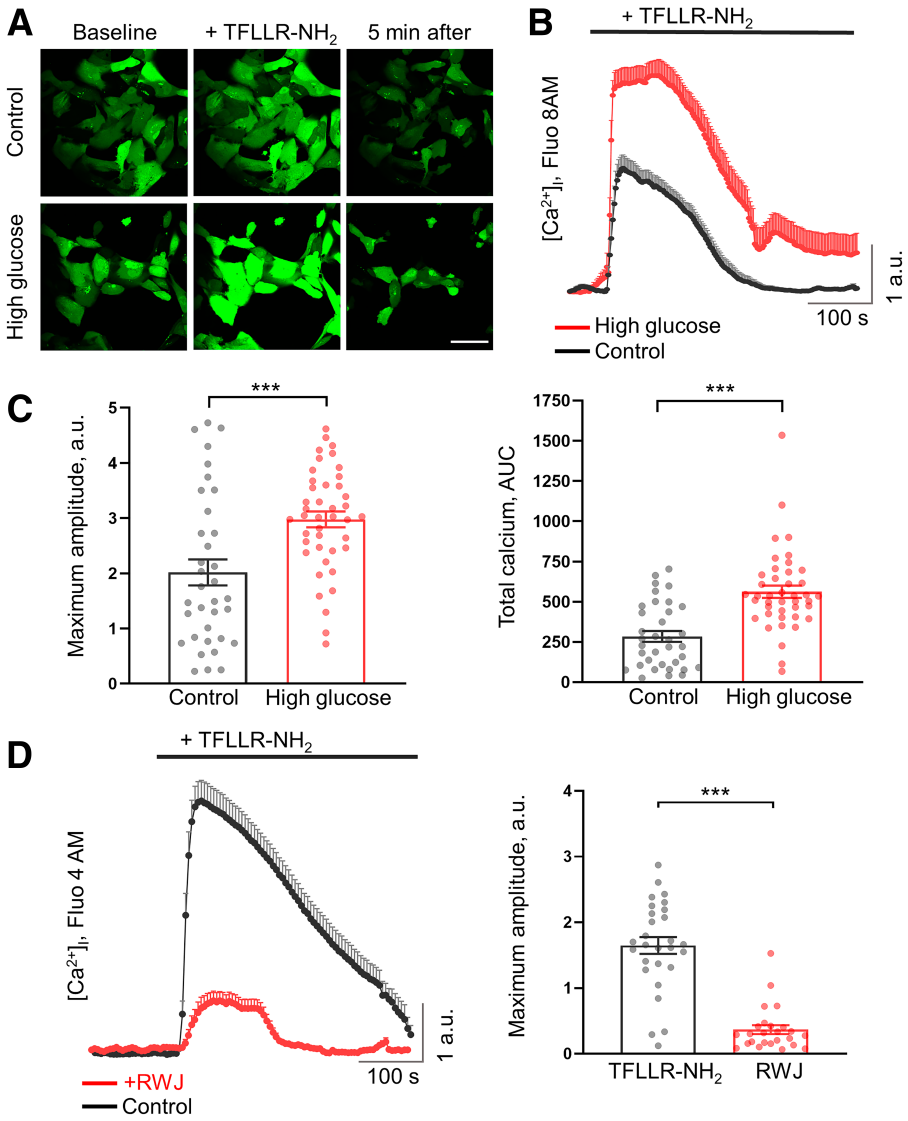

Figure 2—Hyperglycemia-induced increase in PAR1 response in cultured human podocytes. *A*: Representative microphotographs show intracellular calcium ($[Ca^{2+}]_i$) changes (Fluo-8 AM) in response to PAR1 selective agonist TFLLR-NH_2 (10 μmol/L) in control and high-glucose conditions (30 mmol/L for 12 h). Scale bar is 100 μm. *B*: High-glucose–induced significant elevation in $[Ca^{2+}]_i$ response to PAR1 activation (red line) to compare with control (black line); a.u., arbitrary units. *C*: The statistical summary shows the maximum amplitude and total calcium (area under the curve [AUC] in individual podocytes ($n \geq 35$ for each group, *t* test, ***$P < 0.001$). *D*: Changes in intracellular calcium after PAR1 agonist application (TFLLR-NH_2, 10 μmol/L) in the presence or absence of PAR1 receptor blocker RWJ 56100 (5 μmol/L). The statistical summary shows a significant difference between the maximum amplitude of the control response and the response with the presence of RWJ ($n \geq 25$ cells, *t* test, ***$P < 0.001$).

TRPC6 expression. Activation of PAR1 with TFLLR-NH_2 also caused time-dependent changes in p-ERK1/2 and PLC-γ1.

Acute Application of Serine Proteases in T2DN Rat Glomeruli Promotes Activation of Intracellular Calcium in Podocytes

To evaluate changes in $[Ca^{2+}]_i$ levels in response to serine proteases under the setting of DN, we conducted live-cell Ca^{2+} fluorescence imaging experiments in podocytes of isolated rat glomeruli. Changes in $[Ca^{2+}]_i$ in response to acute applications of thrombin or urokinase were tested in glomerular podocytes from Wistar and T2DN rats. Figure 5*A* shows representative images of the glomerulus from a T2DN rat loaded with fluorescent dye before and after thrombin application. The experiment confirmed our data in human podocyte culture and revealed a rapid elevation in Ca^{2+} in response to PAR receptor activation. Importantly, diabetic rats exhibit a significantly higher response to thrombin (Fig. 5*B*). Moreover, the plasma concentration of thrombin in T2DN animals was significantly elevated compared with Wistar (Fig. 5*C*). In addition, we evaluated changes in calcium dynamics in response to acute urokinase application. Urokinase produced rapid transient activation of $[Ca^{2+}]_i$ in podocytes,

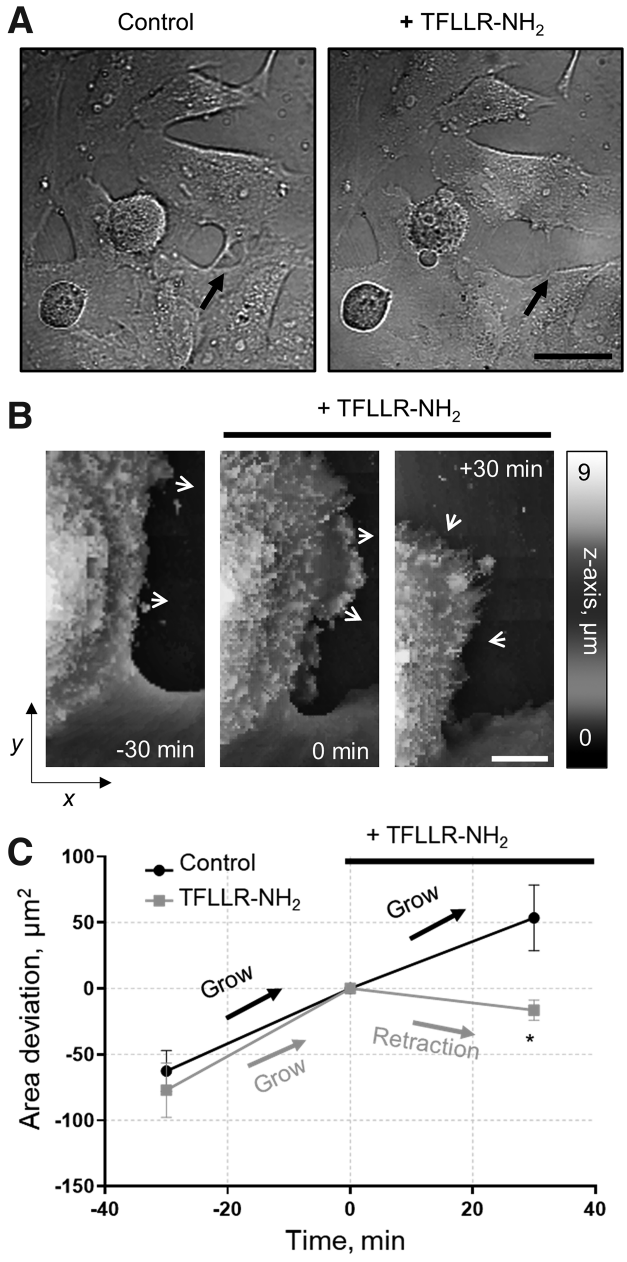

Figure 3—PAR1-mediated remodeling of podocyte structures. *A*: Representative light microscopy imaging of PAR1-mediated remodeling of tight junctions in cultured human podocytes after TFLLR-NH_2 (20 μmol/L) application. Scale bar is 50 μm. *B*: Effect of PAR1 receptor agonist TFLLR-NH_2 on podocyte structures assessed with SICM. An example of podocyte lamellipodia before and after application of TFLLR-NH_2 (20 μmol/L). The arrows show the direction of lamellipodium changes over time. Scale bar is 5 μm. *C*: Summary graph demonstrating that activation of PAR1 signaling promotes retraction of podocyte lamellipodium. Data are shown as a cell area deviation normalized to the time of TFLLR-NH_2 application (0 min). The graph demonstrates significant retraction of the lamellipodium and a significant decrease in cell surface area ($n = 5$, t test, $P < 0.05$). The arrows show the direction of lamellipodium changes over time.

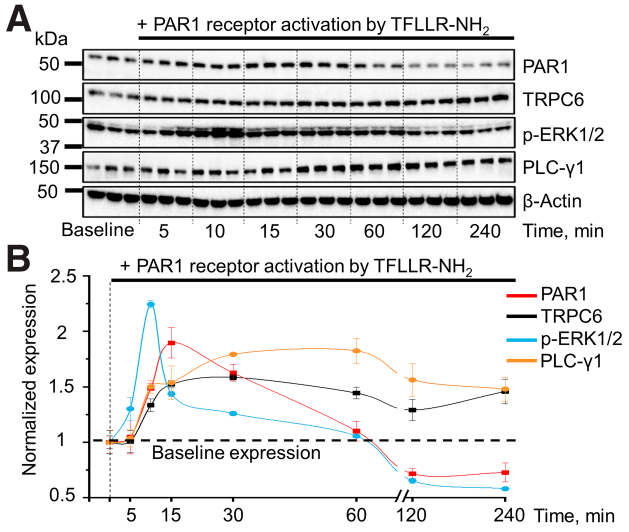

Figure 4—Downstream signaling changes in cultured human podocytes after PAR1 activation. Stimulation of PAR1 receptor cascade by the specific peptide TFLLR-NH_2 promotes time-dependent remodeling in intracellular signaling pathways of the cultured human podocytes. *A*: Western blot analysis of PAR1, TRPC6, p-ERK1/2, and PLC-γ1 in cultured human podocytes following activation of PAR1 signaling. *B*: The summary of time-dependent changes in PAR1 and TRPC6 expression in podocytes stimulated by the 10 μmol/L TFLLR-NH_2. Data were normalized to the baseline expression level of the corresponding pathway before PAR1 activation.

as shown in Fig. 5*D*. A summary graph shows $[Ca^{2+}]_i$ increase in response to 0.1 and 2.7 mg/mL urokinase application. Also, old male T2DN rats exhibit significantly elevated urinary urokinase levels compared with young T2DN and Wistar control rats (Fig. 5*E*), confirming that late-stage DKD is associated with increases in serine protease levels. Old T2DN female rats had significantly higher thrombin compared with Wistar control rats. Interestingly, urokinase levels were significantly lower in old T2DN females than in males, consistent with their less severe renal damage, which has been reported previously (32). It is necessary to consider the possibility that the observed changes in protease levels in our study might be due to aging. Regrettably, we are unable to examine this directly because of a lack of samples from aged Wistar rats for comparison, which serves as a limitation of our study.

To confirm elevated PAR1 expression in the development of DN, we isolated glomerular fractions from control and diabetic animals at different stages of diabetic kidney disease. Thus, analyzed protein levels represent specific glomerulus expression. We included 12-week-old Wistar rats as a nondiabetic control and 12-week-old GK rats as a diabetic control. As shown in Fig. 5*F*, while PAR1 expression in the young T2DN rats is minimal and comparable to GK and Wistar controls, there is a dramatic increase in its expression in old T2DN rats with the later stage of DKD.

PAR-Mediated TRPC6 Activation in Glomerular Podocytes

TRPC6 channels are essential mediators of $[Ca^{2+}]_i$ signaling in podocytes (4). TRPC6 channel opening is predominantly activated through GPCR-mediated cascades, including

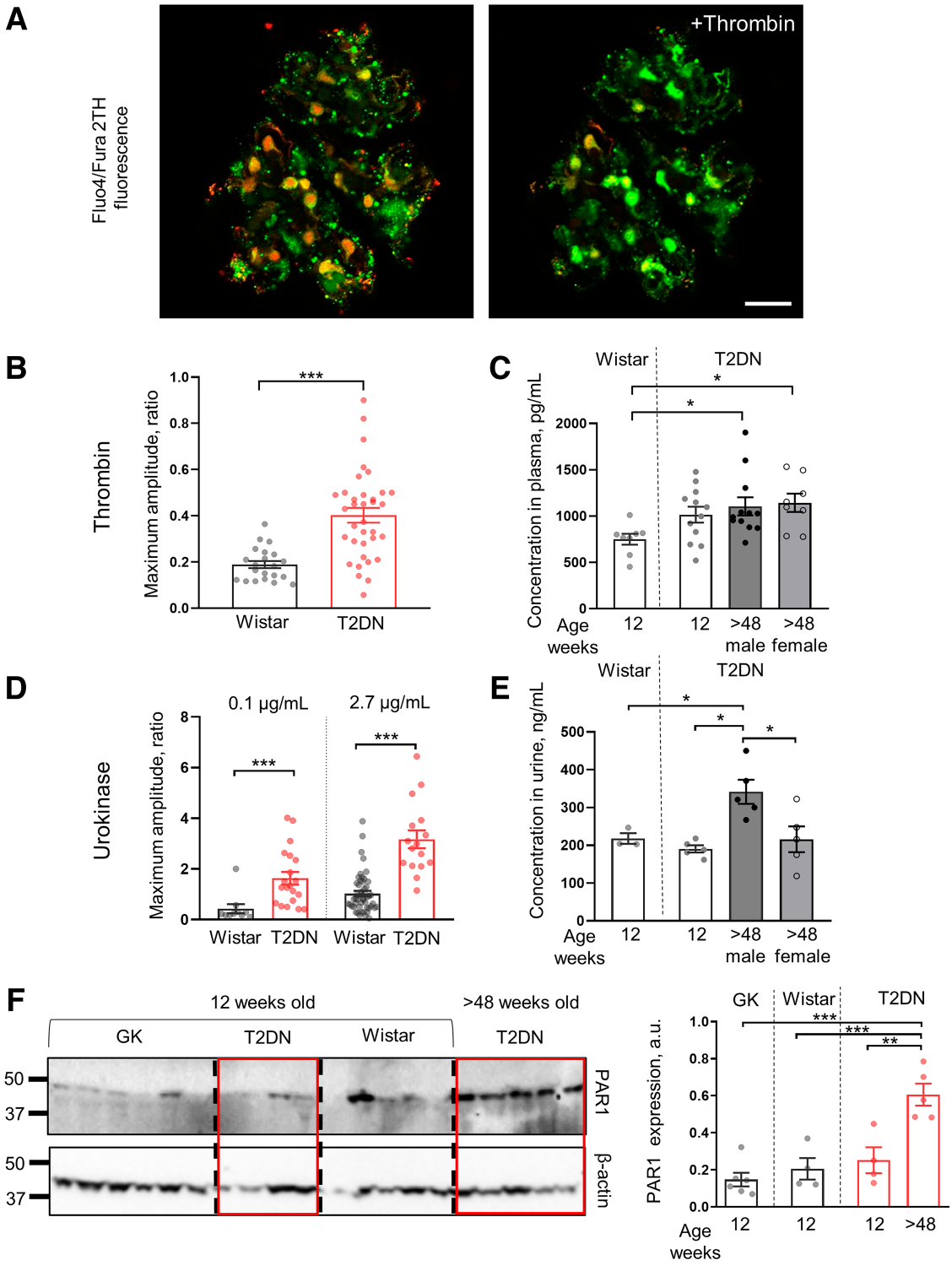

Figure 5—Acute serine protease application promotes activation of intracellular calcium in T2DN rat glomerular podocytes. *A*: The representative confocal imaging showed an application of thrombin (10 µmol/L) and a corresponding elevation of intracellular calcium (3 min between images) indicated as the ratio of Fluo-4 (green) and Fura 2TH (red) fluorescent dyes. Scale bar is 20 µmol/L. *B*: Summary of the $[Ca^{2+}]_i$ amplitudes in response to thrombin in Wistar and T2DN rats ($n \geq 21$, $^{***}P < 0.001$). *C*: Thrombin concentration in plasma of young Wistar ($n = 8$) and T2DN ($n = 12$) rats, and >48-week-old T2DN male ($n = 12$) and female ($n = 8$) rats (ANOVA, $^{*}P < 0.05$). *D*: Summary of the $[Ca^{2+}]_i$ amplitudes in response to different concentrations of urokinase in Wistar and T2DN rats (0.1 µg/mL, Wistar $n = 10$ vs. T2DN $n = 20$ cells, *t* test, $^{***}P < 0.001$; 2.7 µg/mL, Wistar $n = 51$ vs. T2DN $n = 16$ cells, *t* test, $^{***}P < 0.001$). *E*: Urokinase concentration in urine of 12-week-old Wistar and 12- and 48-week-old male and 48-week-old female T2DN rats (ANOVA, $^{*}P < 0.05$). *F*: Western blot analysis of PAR1 expression in GK ($n = 6$), Wistar ($n = 4$), and young ($n = 4$) and old ($n = 5$) T2DN rats. Each band represents a fraction of freshly isolated glomeruli from one rat. Data are mean ± SEM, ANOVA, $^{**}P < 0.01$, $^{***}P < 0.001$; a.u. arbitrary units.

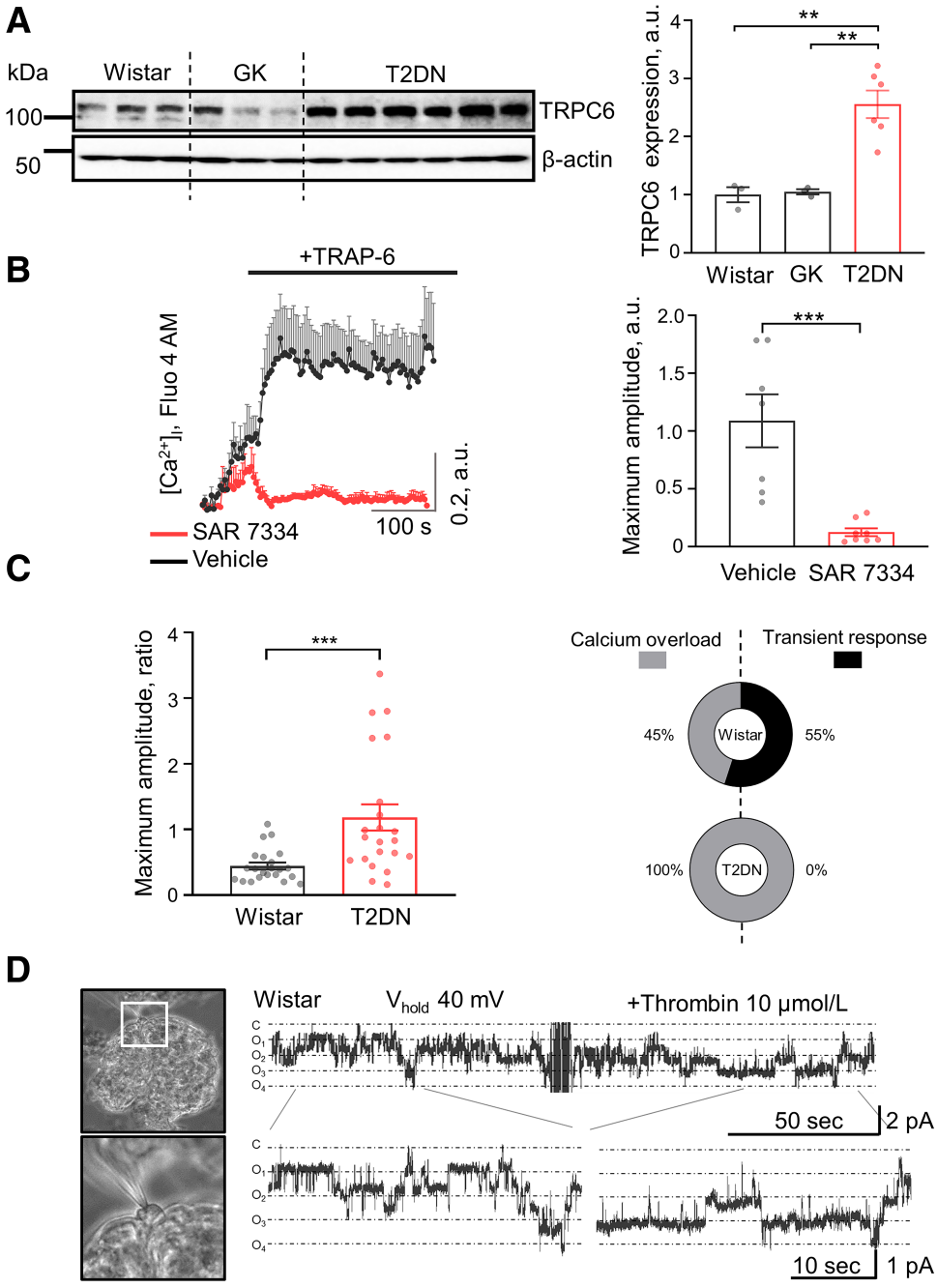

Figure 6—PAR-mediated TRPC6 activation. *A*: The progression of DN in T2DN rats (>48 weeks old) strongly correlates with increased TRPC6 expression (Wistar $n = 3$ vs. GK $n = 3$ vs. T2DN $n = 6$; mean ± SEM, ANOVA, $^{**}P < 0.01$); a.u., arbitrary units. *B*: Changes in $[Ca^{2+}]_i$ in podocytes of freshly isolated glomeruli activated by acute application of selective PAR1 agonist TRAP-6 (10 µmol/L) after 10 min of preincubation with vehicle (DMSO; black) or TRPC6 blocker (20 µmol/L, SAR7334; red). The summary shows changes in maximum fluorescence amplitude (Fluo-4 AM) in response to PAR1 activation rat freshly isolated glomeruli ($n \geq 7$, *t* test, $^{***}P < 0.001$). *C*: The maximum amplitude ratio of $[Ca^{2+}]_i$ response in the podocyte of the freshly isolated glomerulus after PAR1 activation by TRAP-6 (10 µmol/L) was significantly higher in T2DN rats compared with Wistar ($n \geq 22$, *t* test, $^{***}P < 0.001$). In Wistar rats, both fast and slow calcium responses were observed (55% vs. 45%, respectively), but, in T2DN rats, only a slow, sustained response was present. *D*: Thrombin activates TRPC-like channels in the podocytes of the freshly isolated rat glomeruli from the Wistar rat. Microphotograph of the patch clamp experiment on the podocyte of the freshly isolated glomerulus (the white rectangle highlights the specified area shown on the photo below, showcasing the details of the patch-clamp procedure on the podocyte) and representative current trace from a cell. The application of thrombin (10 µmol/L) promoted a transient increase in channel activity. The close state is indicated as "c," and the open state is indicated as "o."

Angiotensin II receptor and κ-opioid receptor signaling in podocytes (24,33). As was described above, cultured human podocytes increase TRPC6 expression in response to PAR1 activation (Fig. 4). Here we used isolated glomeruli to reveal PAR1/TRPC6-mediated Ca^{2+} influx in podocytes in the setting of DN. Western blot analysis revealed that TRPC6

expression is increased in T2DN but not Wistar or GK rats (Fig. 6*A*). These data demonstrate a strong correlation between the progression of DN and the increase in TRPC6 expression.

To investigate TRPC6 contributions to PAR1-mediated calcium response, we conducted calcium imaging experiments in freshly isolated glomeruli from T2DN rats. The application of PAR1 agonist (TRAP-6) promoted the sustained elevation of $[Ca^{2+}]_i$ in isolated glomeruli from T2DN rats (Fig. 6*B*). This response was blunted in the presence of SAR7334, a specific TRPC6 inhibitor. Additionally, similar to the ratiometric calcium imaging experiments, we observed high and sustained TPRC6 single-channel activation in response to PAR1 stimulation in podocytes. Figure 6*D* illustrates a representative activity of endogenous TRPC6 channels following the addition of thrombin (10 μmol/L). There is considerable evidence that the absence of a normal transient calcium response correlates with pathological conditions. The duration of calcium influx determines whether cells survive or die by apoptosis or necrotic lysis (34,35). In podocytes of freshly isolated glomeruli from Wistar rats, we observed both transient and sustained calcium level changes in response to the acute application of TRAP-6 (Fig. 6*C*). However, in T2DN rats, we observed only slow, sustained activation. Moreover, the amplitude of the $[Ca^{2+}]_i$ response was significantly higher in T2DN rats than in Wistar rats.

T2DN$^{PAR1+/-}$ Rats Have Attenuated Development of Microalbuminuria and Glomerular Damage

To test our hypothesis in vivo, we genetically ablated PAR1 using CRISPR/Cas9 gene editing on the T2DN rat background. The deletion eliminates functional PAR1 expression. We used heterozygous rats in our study, as the homozygous rats were embryonically lethal. mRNA expression of PAR1 estimated by RT–quantitative PCR in >48-week-old T2DN$^{Par1+/-}$ rats was significantly compared with T2DN rats (Supplementary Fig. 3). We determined the physiological consequences of knocking out PAR1 in T2DN rats by examining the renal function and the progression of DN complications (Fig. 7). The attenuation of glomerular pathology and damage is suggested by significantly lower albuminuria in T2DN$^{Par1+/-}$ rats (Fig. 7*A*). Blood electrolytes analysis showed no difference between groups, confirming the comparable progression of diabetes (Supplementary Tables 1 and 2). Moreover, we found significantly attenuated glomerular injury in T2DN$^{Par1+/-}$ compared with T2DN rats. Semiquantitative morphometric analysis of glomerular injury score revealed a significant decline in glomerular pathology in T2DN$^{Par1+/-}$ rats, with only 7% of T2DN$^{Par1+/-}$ glomeruli having the most severe injury score compared with 24% of T2DN (Fig. 7*B*). Other clinically associated glomerular damages were attenuated in T2DN$^{Par1+/-}$. Capillary microaneurysm, prominent thickening of the basement membrane, glomerular nodules, and glomerular hyalinosis were relativity lower, by 12%, 35%, 50%, and 14%, respectively (Fig. 7*C*–*E*).

DISCUSSION

In this study, we present compelling evidence that serine proteases and PAR1 signaling are involved in the development of DN via TRPC6-mediated intracellular calcium signaling (Fig. 8). Different disorders and pathologies can provoke coagulation cascade activity and increase endogenous proteases' levels. Multiple clinical studies reported that increasing serine protease activity, particularly thrombin, is associated with DN (36–38). We found that T2DN rats exhibit significantly elevated urinary urokinase levels and increased expression of PAR1, which supports previous findings that PAR1 can be involved in normal and pathological processes in the kidney (11,14). Furthermore, we demonstrated that activation of PAR1 by serine proteases or pharmacological agents activates TRPC6 channels and leads to prolonged elevated calcium flux in podocytes. Previous studies focused on PAR1 signaling in type 1 diabetes, and models of nephropathy demonstrated the role of PAR1 in podocyte damage, as well as the renoprotective effects of blocking PAR1 in type 1 diabetes (18,19,39). Thus, our studies confirmed previously established mechanisms. Furthermore, the current studies examined PAR1 signaling in the context of type 2 diabetes, which has never been explored. To address the significance of this pathway and uncover potential mechanisms, we have generated a novel PAR1 knockout rat model on a genetic type 2 diabetic background (T2DN$^{Par1+/-}$). Our results provide strong evidence that heterozygous mutation of PAR1 in T2DN rats attenuates the development of microalbuminuria and glomerular damage. This therapeutic effect could be caused by decreasing extensive calcium signaling in podocytes due to the loss of PAR1.

PAR1 has a complex, context-specific G-protein signaling involved in various cellular processes, including calcium level management and cytoskeleton rearrangement (40,41). This knowledge is consistent with our findings that serine proteases and pharmacological agents promote activation of PAR1 in podocytes, which triggers a rapid elevation of $[Ca^{2+}]_i$ and leads to the remodeling of podocytes' structure. Also, our data demonstrate the functional presence of PAR1-GPCR signaling in rat and human podocytes, which is increased under diabetic conditions. Furthermore, it was reported that PAR1 antagonism ameliorates podocyte injury in a mouse model of nephropathy via TRPC-mediated elevation of $[Ca^{2+}]_i$ (18). Our experiments with specific TRPC6 blockers confirmed that this type of channel is involved in the PAR1-mediated calcium response. This agrees with the common consensus that TRPC channels are mostly potentiated by tyrosine kinase receptor-mediated activation of phospholipase C or GPCR pathways (42). Further, our studies have revealed that these signaling pathways are highly upregulated in T2DN rats.

Interestingly, a prolonged high level of serine proteases could lead to constitutively active PAR-mediated signaling cascades (43–45). In our experiments, we observed slow, sustained calcium activation in T2DN animals, probably resulting from the continuous activation of TRPC6 channels.

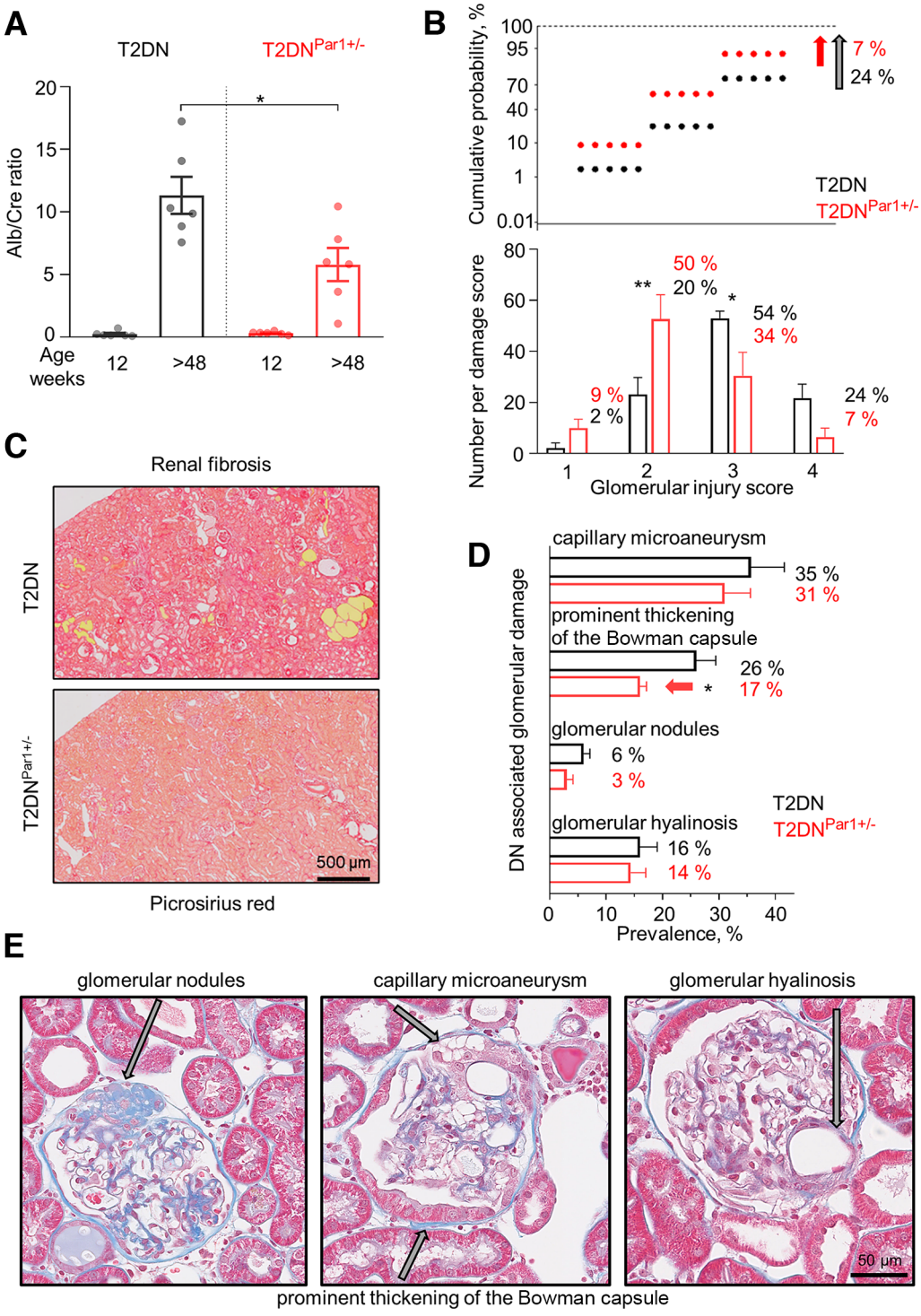

Figure 7—Attenuated development of microalbuminuria and glomerular damage in T2DN$^{PAR1+/-}$ rats. *A*: The progression of albuminuria was significantly lower in old T2DN$^{PAR1+/-}$ rats (24-h metabolic cages/urinary albumin normalized to creatinine, $n = 6$ each group, two-way ANOVA, $^*P < 0.05$, factor 1: 12 vs. 48 weeks of age, factor 2: T2DN vs. T2DN$^{PAR1+/-}$). *B*: The glomerular injury score (0–4, where 0 denotes no damage) was assessed by semiquantitative morphometric analysis for >48-week-old T2DN$^{PAR1+/-}$ and T2DN rats. (top) The cumulative probability distributions of the obtained glomerular scores. (bottom) Numbers of glomeruli per score are shown on the *y* axes. The percentage of glomeruli within the selected score range defined from cumulative distribution is shown. The prevalence of observed glomerular damage was clinically associated with DN in both groups ($n \geq 100$, $N \geq 3$, two-way ANOVA, $^*P < 0.05$, $^{**}P < 0.015$). Note relativity attenuation in the presence of glomerular pathology in T2DN$^{PAR1+/-}$ rats (*D*). Results show a significant decrease in the prominent thickening of basement membrane (*t* test, $^*P < 0.05$), while other parameters exhibit a noticeable, yet nonsignificant trend toward reduction: capillary microaneurysm (35% vs. 31%; reduction 12%); glomerular nodules (6% vs. 3%; reduction 50%); glomerular hyalinosis (16% vs. 14%; reduction 13%). *C*: Renal fibrosis obtained by picrosirius red staining correlates with a significant decrease in kidney injury markers shown above. *E*: Masson trichrome-stained images show examples of glomerular damage in T2DN rats, as indicated by arrows.

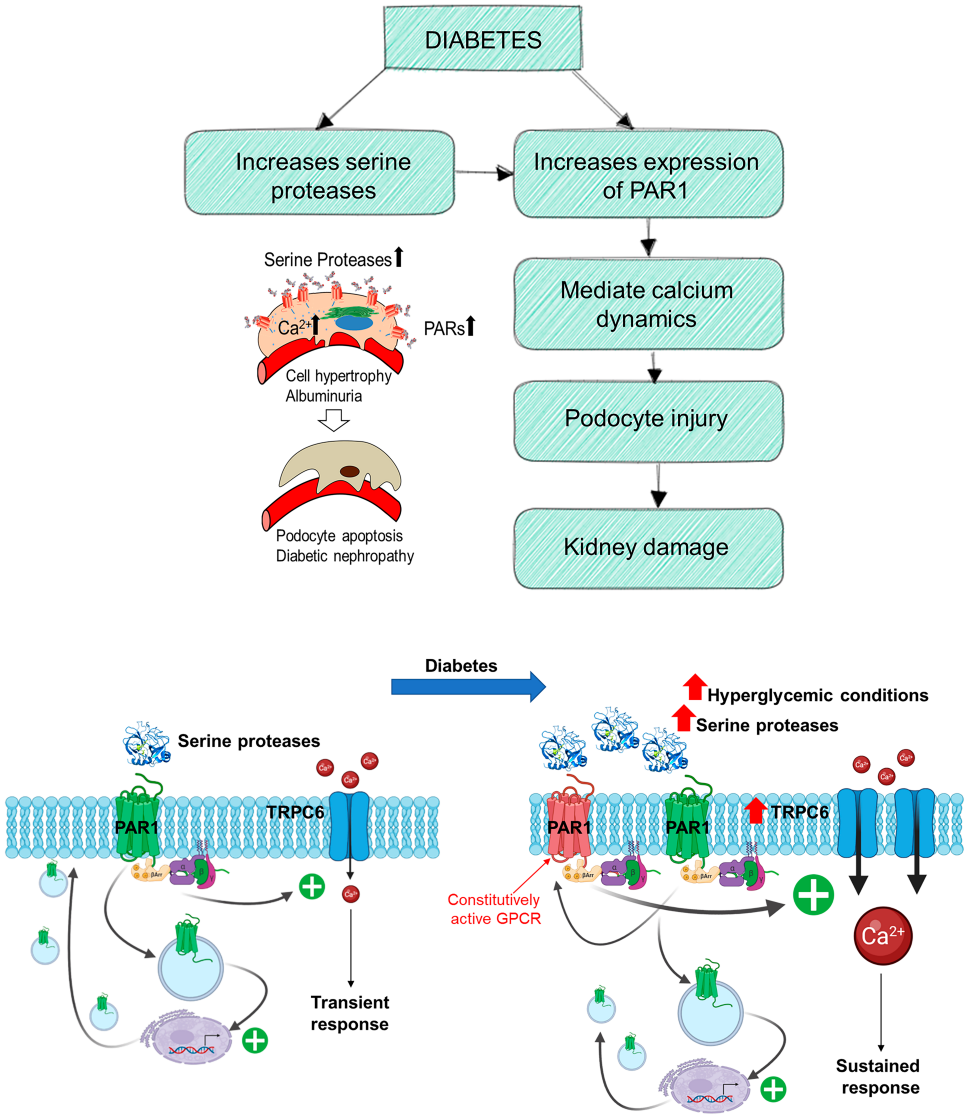

Figure 8—The proposed PAR1-mediated signaling cascade in the diabetic kidney's podocytes. Serine proteases, like thrombin, cause proteolytic cleavage of PAR1 and further activation of intracellular signaling in glomerular podocytes. The signaling mechanism, mediated by the canonical G protein coupling or engagement of β-arrestin–dependent pathways, promotes rapid transient calcium influx through TRPC6 channels. Diabetic disease, characterized by marked elevation of serine proteases and hyperglycemia, causes constitutive activation of PAR1, stimulates TRPC6 activity and expression, and leads to calcium overload and subsequent podocyte injury.

Previous studies reported the possibility of PAR signaling leading to a sustained increase in $[Ca^{2+}]_i$ through the activation of ion channels (46). One of the proposed constitutively active GPCR pathways is mediated by β-arrestin (47). The recruitment of β-arrestins plays an essential role in the internalization or accumulation of the PAR1 receptor on the cell surface. It was also shown that PARs could induce β-arrestin–dependent endosomal ERK1/2 signaling in the cytoplasm (48). We found time-dependent changes in p-ERK1/2 and PLC-γ1 expression following PAR1 activation, which may be involved in the sustained calcium response in podocytes resulting from constitutive activation of GPCR. Evidence suggests that ERK may play a role in the upregulation of TRPC6 expression. A study by Yu et al. (49) demonstrated the possible involvement of ERK in TRPC6 upregulation in the context of TGF-β1–induced podocyte injury. The authors showed that TGF-β1 induced significant activation of p-ERK, and ERK inhibitor reduced the increment of TRPC6 protein and the flux of cytosolic free calcium. This observation implies that ERK may play a role in the upregulation of TRPC6 protein expression in this specific context.

Most of the current studies of PAR signaling pathways in diabetes focus on type 1 diabetes mellitus using STZ models (15,50). Also, most of these studies used PAR-deficient mice. Here, we demonstrate that rats with T2DN background with PAR1 knockout are a valuable model for studying the role of PAR1 in DKD development and, in the future, could be used for studying PARs signaling pathways in vivo. Our experiments with the $T2DN^{Par1+/-}$ animal

model support the hypothesis that PAR1 contributes to the development of albuminuria and glomeruli damage. These results expand previous findings that PAR1-deficient mice had a reduction in proliferation and fibronectin deposition (15) in STZ-induced DN and presented less kidney damage and fibrin deposits in experimental glomerulonephritis (51). It is important to highlight the difference between homozygous PAR1 knockout between species and models. Homozygous PAR1 knockout mice are viable, but it was not the case with homozygous $T2DN^{PAR1-/-}$ rats. This difference may originate from species- or model-specific variations in PAR1 function during development. In T2DN rats, PAR1 may have a more critical function during embryogenesis, which is not as essential in the nondiabetic mouse model. Furthermore, it should be noted that potential pitfalls exist when using $T2DN^{Par1+/-}$ rats because they are heterozygous rats, and they might not have as profound a phenotype as the $T2DN^{Par1-/-}$ rats. However, there is mounting evidence that heterozygous models (both mice and rats) with reduced but not abolished protein functions can provide models with greater relevance to the genetics of human disorders (52,53).

In conclusion, these data support our hypothesis that, in conditions of elevated levels of serine proteases during the development of DN, overstimulation of PARs promotes excessive $[Ca^{2+}]_i$ levels in podocytes, ultimately leading to podocyte apoptosis, development of albuminuria, and glomeruli damage. This study provides fundamental knowledge that can be used to develop efficient therapeutic approaches based on PAR and the corresponding serine proteases as potential therapeutic targets to prevent or slow the progression of DKDs. Future work should focus on identifying the molecular mechanisms underlying the activation of PAR-mediated signaling and understanding how these pathways regulate podocyte damage and DN development.

Acknowledgments. The authors thank Christine Duris and Tanya Bufford (Histology Core) for assistance with immunohistochemistry experiments and Dr. Suresh Kumar (Imaging Core) for help with image scanning (all from Medical College of Wisconsin Children's Research Institute). We also thank Dr. Mykhailo Fedoriuk (Medical University of South Carolina) for his help with calcium imaging.

Funding. This work was supported by National Institutes of Health grants R01 DK129227 (to A.S. and O.P.), R35 HL135749, R21 DK129882, R01 DK135644 (to A.S.), and R01 DK126720 (to O.P.); Department of Veteran Affairs grant I01 BX004024 (to A.S.); endowed funds from the SC SmartState Centers of Excellence (to O.P.); and the American Physiological Society Postdoctoral Fellowship (to R.B.).

Duality of Interest. No potential conflicts of interest relevant to this article were reported.

Author Contributions. S.K., O.P., and A.S. designed experiments. R.B., S.K., V.L., M.St., M.Se., O.K., E.I., C.A.K., and O.P. performed experiments, analyzed the results, and prepared data for publication. A.M.G. created the rat model. R.B. prepared the original draft. V.L., O.K., E.I., C.A.K., O.P., and A.S. reviewed and edited the manuscript. O.P. and A.S. supervised the study. All authors reviewed, revised, and approved the article. A.S. is the guarantor of this work and, as such, had full access to all the data in the study and takes responsibility for the integrity of the data and the accuracy of the data analysis.

Prior Presentation. Parts of this study were presented at the Experimental Biology 2022 Meeting, Philadelphia, PA, 2–5 April 2022, and Hypertension 2021, virtual meeting, 27–29 September 2021.

References

1. Johansen KL, Chertow GM, Foley RN, et al. US Renal Data System 2020 Annual Data Report: epidemiology of kidney disease in the United States. Am J Kidney Dis 2021;77(Suppl. 1):A7–A8
2. Thurlow JS, Joshi M, Yan G, et al. Global epidemiology of end-stage kidney disease and disparities in kidney replacement therapy. Am J Nephrol 2021;52:98–107
3. Tervaert TW, Mooyaart AL, Amann K, et al.; Renal Pathology Society. Pathologic classification of diabetic nephropathy. J Am Soc Nephrol 2010;21:556–563
4. Staruschenko A, Ma R, Palygin O, Dryer SE. Ion channels and channelopathies in glomeruli. Physiol Rev 2023;103:787–854
5. Molitoris BA, Sandoval RM, Yadav SPS, Wagner MC. Albumin uptake and processing by the proximal tubule: physiological, pathological, and therapeutic implications. Physiol Rev 2022;102:1625–1667
6. Comper WD, Hilliard LM, Nikolic-Paterson DJ, Russo LM. Disease-dependent mechanisms of albuminuria. Am J Physiol Renal Physiol 2008;295:F1589–F1600
7. Burford JL, Villanueva K, Lam L, et al. Intravital imaging of podocyte calcium in glomerular injury and disease. J Clin Invest 2014;124:2050–2058
8. Kanno Y, Ishisaki A, Kawashita E, Kuretake H, Ikeda K, Matsuo O. uPA attenuated LPS-induced inflammatory osteoclastogenesis through the plasmin/PAR-1/Ca(2+)/CaMKK/AMPK axis. Int J Biol Sci 2016;12:63–71
9. Mills IH. The renal kallikrein-kinin system and sodium excretion. Q J Exp Physiol 1982;67:393–399
10. Chang SS. Albuminuria and diabetic nephropathy. Pediatr Endocrinol Rev 2008;5(Suppl. 4):974–979
11. Madhusudhan T, Kerlin BA, Isermann B. The emerging role of coagulation proteases in kidney disease. Nat Rev Nephrol 2016;12:94–109
12. Bae JS, Kim IS, Rezaie AR. Thrombin down-regulates the TGF-beta-mediated synthesis of collagen and fibronectin by human proximal tubule epithelial cells through the EPCR-dependent activation of PAR-1. J Cell Physiol 2010;225:233–239
13. Chackalamannil S, Wang Y, Greenlee WJ, et al. Discovery of a novel, orally active himbacine-based thrombin receptor antagonist (SCH 530348) with potent antiplatelet activity. J Med Chem 2008;51:3061–3064
14. Rinschen MM, Huesgen PF, Koch RE. The podocyte protease web: uncovering the gatekeepers of glomerular disease. Am J Physiol Renal Physiol 2018;315:F1812–F1816
15. Waasdorp M, Duitman J, Florquin S, Spek CA. Protease-activated receptor-1 deficiency protects against streptozotocin-induced diabetic nephropathy in mice. Sci Rep 2016;6:33030
16. Jean-Charles PY, Kaur S, Shenoy SK. G protein-coupled receptor signaling through β-arrestin-dependent mechanisms. J Cardiovasc Pharmacol 2017;70:142–158
17. Kim H, Kim J, Jeon JP, et al. The roles of G proteins in the activation of TRPC4 and TRPC5 transient receptor potential channels. Channels (Austin) 2012;6:333–343
18. Guan Y, Nakano D, Zhang Y, et al. A protease-activated receptor-1 antagonist protects against podocyte injury in a mouse model of nephropathy. J Pharmacol Sci 2017;135:81–88
19. May CJ, Chesor M, Hunter SE, et al. Podocyte protease activated receptor 1 stimulation in mice produces focal segmental glomerulosclerosis mirroring human disease signaling events. Kidney Int 2023;104:P265–P278
20. Madhusudhan T, Ghosh S, Wang H, et al. Podocyte integrin-β_3 and activated protein C coordinately restrict RhoA signaling and ameliorate diabetic nephropathy. J Am Soc Nephrol 2020;31:1762–1780

21. Palygin O, Spires D, Levchenko V, et al. Progression of diabetic kidney disease in T2DN rats. Am J Physiol Renal Physiol 2019;317:F1450–F1461
22. Palygin O, Levchenko V, Ilatovskaya DV, et al. Essential role of Kir5.1 channels in renal salt handling and blood pressure control. JCI Insight 2017;2:e92331
23. Isaeva E, Fedoriuk M, Bohovyk R, et al. Vibrodissociation method for isolation of defined nephron segments from human and rodent kidneys. Am J Physiol Renal Physiol 2019;317:F1398–F1403
24. Ilatovskaya DV, Palygin O, Chubinskiy-Nadezhdin V, et al. Angiotensin II has acute effects on TRPC6 channels in podocytes of freshly isolated glomeruli. Kidney Int 2014;86:506–514
25. Saleem MA, O'Hare MJ, Reiser J, et al. A conditionally immortalized human podocyte cell line demonstrating nephrin and podocin expression. J Am Soc Nephrol 2002;13:630–638
26. Rogacka D, Piwkowska A, Audzeyenka I, Angielski S, Jankowski M. Involvement of the AMPK-PTEN pathway in insulin resistance induced by high glucose in cultured rat podocytes. Int J Biochem Cell Biol 2014;51:120–130
27. Ilatovskaya DV, Palygin O, Levchenko V, Staruschenko A. Single-channel analysis and calcium imaging in the podocytes of the freshly isolated glomeruli. J Vis Exp 2015;100:e52850
28. Ilatovskaya DV, Palygin O, Levchenko V, Endres BT, Staruschenko A. The role of angiotensin II in glomerular volume dynamics and podocyte calcium handling. Sci Rep 2017;7:299
29. Shalygin A, Shuyskiy LS, Bohovyk R, Palygin O, Staruschenko A, Kaznacheyeva E. Cytoskeleton rearrangements modulate TRPC6 channel activity in podocytes. Int J Mol Sci 2021;22:4396
30. Wang Q, Tian X, Wang Y, et al. Role of transient receptor potential canonical channel 6 (TRPC6) in diabetic kidney disease by regulating podocyte actin cytoskeleton rearrangement. J Diabetes Res 2020;2020:6897390
31. Koshikawa M, Mukoyama M, Mori K, et al. Role of p38 mitogen-activated protein kinase activation in podocyte injury and proteinuria in experimental nephrotic syndrome. J Am Soc Nephrol 2005;16:2690–2701
32. Spires DR, Palygin O, Levchenko V, et al. Sexual dimorphism in the progression of type 2 diabetic kidney disease in T2DN rats. Physiol Genomics 2021;53:223–234
33. Golosova D, Palygin O, Bohovyk R, et al. Role of opioid signaling in kidney damage during the development of salt-induced hypertension. Life Sci Alliance 2020;3:e202000853
34. Choi DW. Calcium: still center-stage in hypoxic-ischemic neuronal death. Trends Neurosci 1995;18:58–60
35. Nicotera P, Orrenius S. The role of calcium in apoptosis. Cell Calcium 1998;23:173–180
36. Ay L, Hoellerl F, Ay C, et al. Thrombin generation in type 2 diabetes with albuminuria and macrovascular disease. Eur J Clin Invest 2012;42:470–477
37. Andersen H, Friis UG, Hansen PB, Svenningsen P, Henriksen JE, Jensen BL. Diabetic nephropathy is associated with increased urine excretion of proteases plasmin, prostasin and urokinase and activation of amiloride-sensitive current in collecting duct cells. Nephrol Dial Transplant 2015;30:781–789
38. Cohen Z, Gonzales RF, Davis-Gorman GF, Copeland JG, McDonagh PF. Thrombin activity and platelet microparticle formation are increased in type 2 diabetic platelets: a potential correlation with caspase activation. Thromb Res 2002;107:217–221
39. Mitsui S, Oe Y, Sekimoto A, et al. Dual blockade of protease-activated receptor 1 and 2 additively ameliorates diabetic kidney disease. Am J Physiol Renal Physiol 2020;318:F1067–F1073
40. Pontarollo G, Mann A, Brandão I, Malinarich F, Schöpf M, Reinhardt C. Protease-activated receptor signaling in intestinal permeability regulation. FEBS J 2020;287:645–658
41. Coughlin SR. Thrombin signalling and protease-activated receptors. Nature 2000;407:258–264
42. Hisatsune C, Kuroda Y, Nakamura K, et al. Regulation of TRPC6 channel activity by tyrosine phosphorylation. J Biol Chem 2004;279:18887–18894
43. Liu X, Yu J, Song S, Yue X, Li Q. Protease-activated receptor-1 (PAR-1): a promising molecular target for cancer. Oncotarget 2017;8:107334–107345
44. Zhao P, Pattison LA, Jensen DD, et al. Protein kinase D and Gβγ mediate sustained nociceptive signaling by biased agonists of protease-activated receptor-2. J Biol Chem 2019;294:10649–10662
45. Sharma R, Waller AP, Agrawal S, et al. Thrombin-induced podocyte injury is protease-activated receptor dependent. J Am Soc Nephrol 2017;28:2618–2630
46. Poole DP, Amadesi S, Veldhuis NA, et al. Protease-activated receptor 2 (PAR2) protein and transient receptor potential vanilloid 4 (TRPV4) protein coupling is required for sustained inflammatory signaling. J Biol Chem 2013;288:5790–5802
47. Paing MM, Stutts AB, Kohout TA, Lefkowitz RJ, Trejo J. β-Arrestins regulate protease-activated receptor-1 desensitization but not internalization or down-regulation. J Biol Chem 2002;277:1292–1300
48. Ge L, Ly Y, Hollenberg M, DeFea K. A beta-arrestin-dependent scaffold is associated with prolonged MAPK activation in pseudopodia during protease-activated receptor-2-induced chemotaxis. J Biol Chem 2003;278:34418–34426
49. Yu L, Lin Q, Liao H, Feng J, Dong X, Ye J. TGF-β1 induces podocyte injury through Smad3-ERK-NF-κB pathway and Fyn-dependent TRPC6 phosphorylation. Cell Physiol Biochem 2010;26:869–878
50. Rahadian A, Fukuda D, Salim HM, et al. Thrombin inhibition by dabigatran attenuates endothelial dysfunction in diabetic mice. Vascul Pharmacol 2020;124:106632
51. Cunningham MA, Rondeau E, Chen X, Coughlin SR, Holdsworth SR, Tipping PG. Protease-activated receptor 1 mediates thrombin-dependent, cell-mediated renal inflammation in crescentic glomerulonephritis. J Exp Med 2000;191:455–462
52. Kalueff AV, Ren-Patterson RF, Murphy DL. The developing use of heterozygous mutant mouse models in brain monoamine transporter research. Trends Pharmacol Sci 2007;28:122–127
53. Zhou X, Zhang Z, Shin MK, et al. Heterozygous disruption of renal outer medullary potassium channel in rats is associated with reduced blood pressure. Hypertension 2013;62:288–294